

NASA TECHNICAL NOTE



NASA TN D-5320

*c. 1*

NASA TN D-5320



LOAN COPY: RETURN TO  
AFWL (WLIL-2)  
KIRTLAND AFB, N MEX

A FABRICATION PROCESS FOR  
GLASS COATED ELECTRON-BOMBARDMENT  
ION THRUSTER GRIDS

*by Bruce A. Banks*

*Lewis Research Center  
Cleveland, Ohio*



A FABRICATION PROCESS FOR GLASS COATED ELECTRON-  
BOMBARDMENT ION THRUSTER GRIDS

By Bruce A. Banks

Lewis Research Center  
Cleveland, Ohio

NATIONAL AERONAUTICS AND SPACE ADMINISTRATION

---

For sale by the Clearinghouse for Federal Scientific and Technical Information  
Springfield, Virginia 22151 - CFSTI price \$3.00

## ABSTRACT

A method was developed for producing nearly bubble-free glass coatings for molybdenum ion thruster accelerator grids. The method involves a helium diffusion process. Grids for 5-, 15-, and 30-cm-diameter thrusters were fabricated and tested. Pertinent grid design criteria and test results are presented.

# A FABRICATION PROCESS FOR GLASS COATED ELECTRON- BOMBARDMENT ION THRUSTER GRIDS

by Bruce A. Banks

Lewis Research Center

## SUMMARY

A method for producing nearly bubble-free glass coatings on ion thruster accelerator grids was developed. Bubbles in the glass were eliminated by a helium diffusion process during the fusing operation. A factor of more than eight improvement in fused glass effective electrical breakdown strength was achieved using this process rather than a conventional fusing process. Consideration was given to the grid geometry and coating thickness limitations as determined by surface tension instabilities. Fused glass composite accelerator grids were successfully fabricated and tested for 5-, 15-, and 30-centimeter-diameter thrusters.

## INTRODUCTION

The accelerator grid system is a main component of an electron bombardment ion thruster. It contains the discharge plasma at the downstream end of the ion chamber and forms the proper ion optics to produce a useful exhaust ion beam (refs. 1 and 2). Preliminary tests of composite accelerator grid systems indicated the possibility of substantial performance gains over conventional double grid systems (refs. 3 and 4). More recent investigations of a fused glass type composite accelerator grid have indicated favorable grid performance provided that electrical breakdown problems can be eliminated.

A composite accelerator grid differs from the conventional two-grid system in that an electrical insulator near or in contact with a metallic accelerator grid replaces the screen grid. The concept is illustrated in figure 1.

Figure 2 is a photograph of a composite accelerator grid of the fused glass type. It consists of a molybdenum grid which has been coated on one side with glass. Briefly the coating process consists of first spraying a slurry of powdered glass and water on one side of the metallic grid. After the water has evaporated, the composite grid is

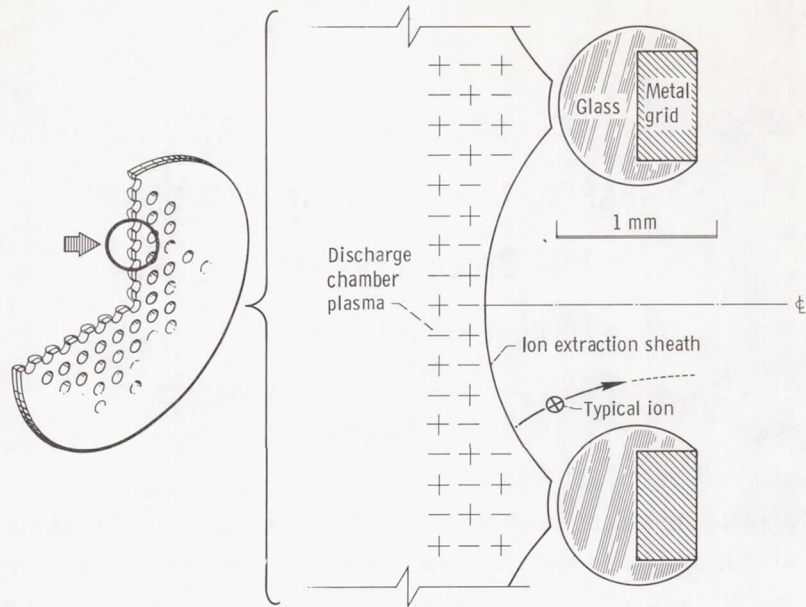


Figure 1. - Section view of glass coated grid concept.

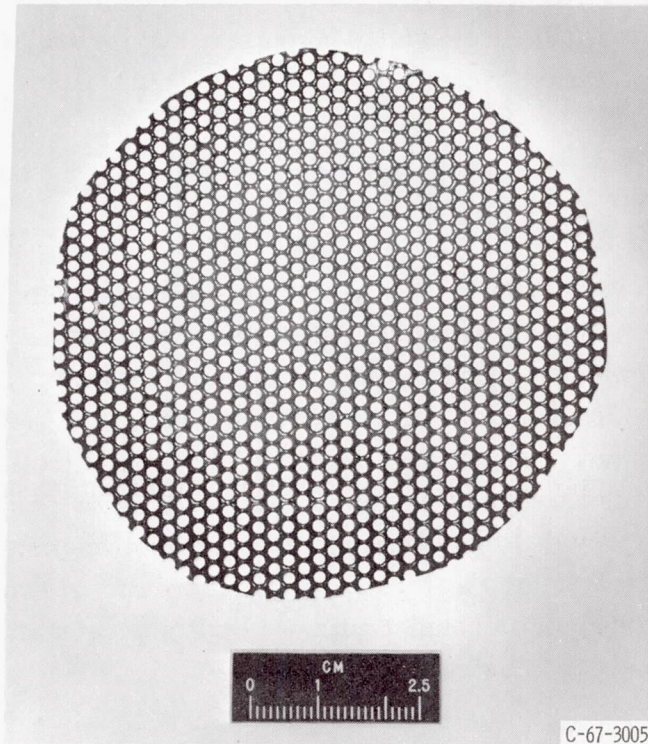


Figure 2. - Fused-glass composite accelerator grid for a 5-centimeter-diameter Kaufman mercury ion thruster. Substrate is prepunched molybdenum sheet.

placed in an oven containing an inert atmosphere and heated to fuse the powdered glass particles together and to the grid.

During thruster operation, a strong electric field is applied across the glass coating. The electrical breakdown strength of the coating can be severely reduced if any large bubbles and/or if numerous small bubbles are present. Figure 3, for example, shows a puncture caused by electrical breakdown of the glass attributed to the presence of bubbles. Breakdown sites in the composite grid are possible causes of increased power losses in the thruster system and in general will lead to degradation in thruster performance.

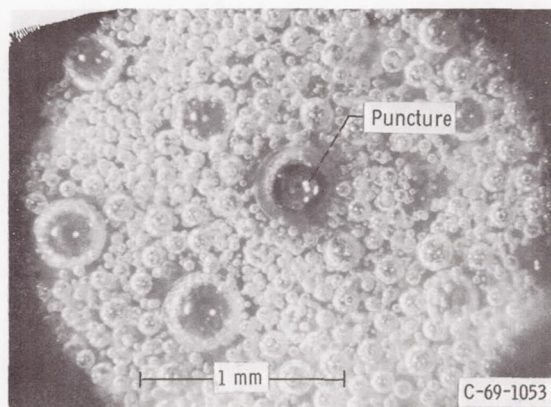


Figure 3. - Electrical breakdown site (looking at glass surface) caused by bubble in 0.43-millimeter-thick Corning glass 7052 coating on molybdenum substrate.

Another possible problem area concerns grid heating. Grid heating can be caused by the thruster cathode thermal radiation, dissipation of the power in the discharge chamber plasma, charge-exchange ion impingement, and the slight conductivity of the insulating material. Because of this, the composite grid electrical insulating material must not degrade at the high temperatures experienced in normal thruster operation.

Elimination of nearly all of the bubbles and reduction of the size of the few remaining bubbles has been found to be possible using a helium diffusion process first discovered by Badger (ref. 5) and conceived independently by the author.

The glass coated grid fabrication technique described in this report employs this process. First, background information is presented to show the effect of bubbles on the coating's breakdown strength and limitations on coating thickness. Then the experimental fabrication technique is described in detail. Finally, data and photographs of experimental results comparing the effects of coating techniques are presented and discussed.

## BACKGROUND

### Effect of Bubbles on Electrical Breakdown Strength

The fused glass coating on a composite accelerator grid is subjected to high electric field strengths when operating in an ion thruster. Electrical breakdown will occur in the glass and degrade the grid performance if the local electrical breakdown strength of the coating is exceeded. It is useful to investigate what effect bubbles have on the local electrical breakdown strength of the glass coating and how the breakdown strength varies with bubbles size. If a bubble of radius  $r_B$  has its center at a distance  $d_s$  from the glass surface (which is exposed to the plasma) and at a distance  $d_m$  from the glass metal interface as depicted in figure 4 then the electric field,  $E_B$ , in the bubble is approximately uniform and given by (refs. 6 and 7).

$$E_B \cong \frac{3\kappa E_g}{2\kappa + 1} \quad (1)$$

provided that  $d_s > 2r_B$  and  $d_m > 2r_B$ . (All symbols are defined in appendix A.) Here

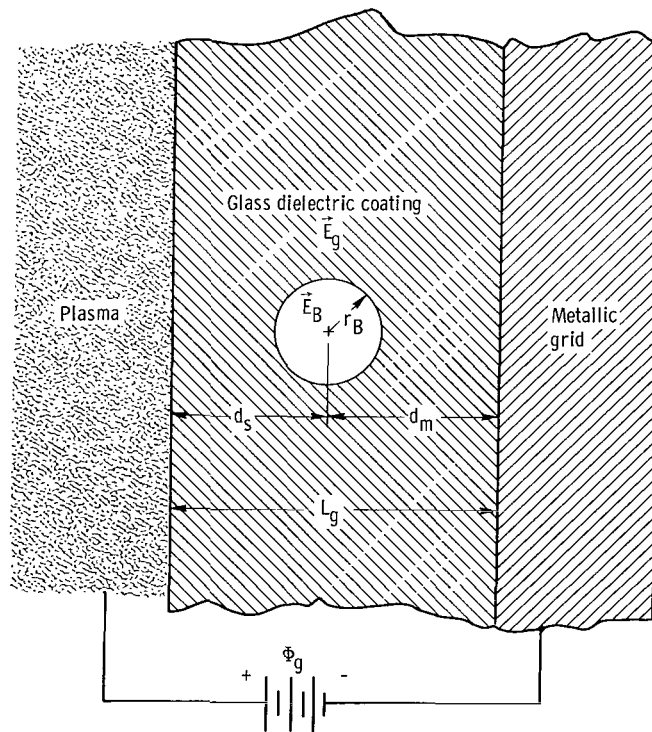


Figure 4. - Bubble in fused-glass coating.

$\kappa$  is the dielectric constant for the glass and  $E_g$ , the electric field in the glass far from the bubble, is given by

$$E_g = \frac{\Phi_g}{d_s + d_m} = \frac{\Phi_g}{L_g} \quad (2)$$

thus

$$E_B \cong \frac{3\kappa\Phi_g}{(2\kappa + 1)L_g} \quad (3)$$

If one increased  $E_B$  by increasing  $\Phi_g$  then eventually electrical breakdown in the bubble will occur. The breakdown potential drop across the bubble  $\Phi_b$  can be found from a Paschen curve for the encapsulated gas relating  $\Phi_b$  as a function of pressure times distance, say  $2r_B$  (see fig. 4). Then the breakdown condition is given approximately as

$$\Phi_b \cong 2r_B E_B$$

Once an electrical discharge occurs within the bubble the conductivity of the plasma formed therein reduces the potential drop across the bubble. As a result, most of the potential drop between the thruster discharge chamber plasma and metallic grid, along a line through the center of the bubble, is through the glass only, so that,

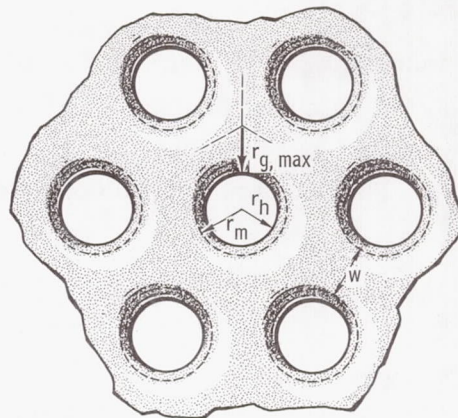
$$E_g \cong \frac{\Phi_g}{L_g - 2r_B} \quad (4)$$

If this new electric field is in excess of the dielectric strength of the glass then electrical breakdown will occur from the mercury plasma through the glass (and bubble) to the metallic grid. Equation (4) indicates that the effective breakdown strength of the glass coating is equivalent to that of a bubble free coating whose thickness approximately  $L_g - 2r_B$ . Thus, bubbles whose diameters are a large fraction of the total coating thickness would severely reduce the maximum potential difference which could be applied across the grid.

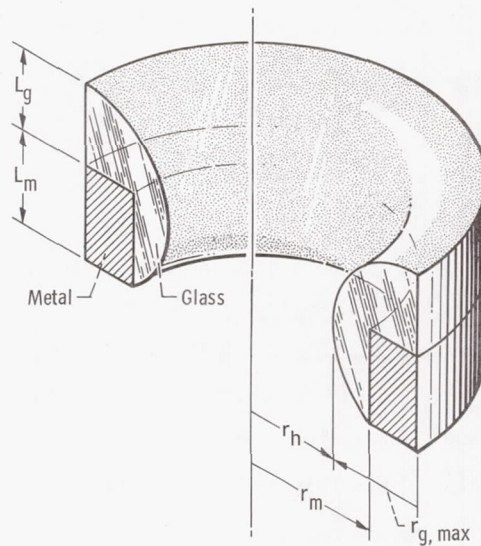
In an actual glass-coated accelerator grid thousands of small bubbles may be present. The collective effect of breakdown of the gas in many bubbles, of course, can also lead to breakdown through the glass.

## Coating Thickness Limitations as Dictated by Hole Wall Stability

One direct approach to prevent electrical breakdown of the glass is to increase the glass coating thickness,  $L_g$ , which will reduce the electric field in the glass for a given applied potential difference  $\Phi_g$ . The glass coating cannot be made arbitrarily thick, however, because the surface tension forces in the molten glass will cause the grid holes to be filled with glass during fabrication. This will occur if the hole radius  $r_h$  is smaller than the maximum coating radius  $r_{g, \max}$ , as depicted in figure 5. (A more detailed treatment of this hole stability consideration is given in appendix B.) At fusing temperatures the hole fill time is much shorter than the fusing time for holes where  $r_h$  is less

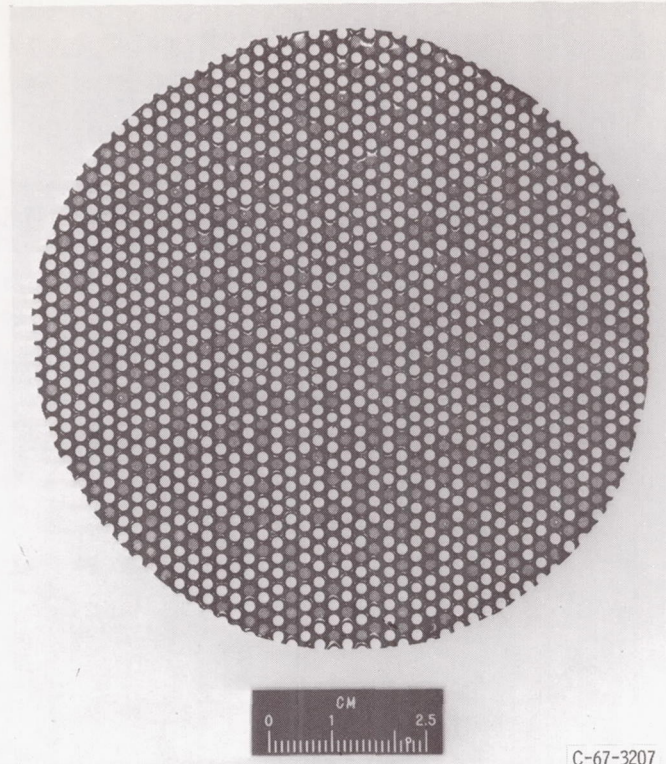


(a) Top view.



(b) Perspective view.

Figure 5. - Fused-glass composite grid parameters.



C-67-3207

Figure 6. - Fused-glass composite grid with a large number of holes filled in with glass due to hole-wall instability.

than  $r_{g, \max}$ . (A representative grid whose hole walls collapsed from this instability is shown in fig. 6.)

The limiting glass coating thickness  $L_{g, \max}$  is dependent only on a metallic hole radius  $r_m$ , metallic grid fraction open area  $F_m$ , and the metallic grid thickness  $L_m$ . As derived in appendix B

$$L_{g, \max} = r_m \sqrt{\frac{\pi}{6F_m \sqrt{3}}} \left[ 1 + \sqrt{1 - \left( 2 - \sqrt{\frac{6F_m \sqrt{3}}{\pi}} \right)^2} \right] - L_m \quad (5)$$

for  $F_m > \pi / (6\sqrt{3}) \cong 0.3027$ . A plot of  $(L_{g, \max} + L_m) / r_m$  as a function of  $F_m$  is shown in figure 7.

Thus, the electric field in the glass can be reduced by increasing glass thickness in order to minimize electrical breakdown caused by the presence of bubbles but the maximum glass coating thickness is limited by hole wall stability considerations. However, a

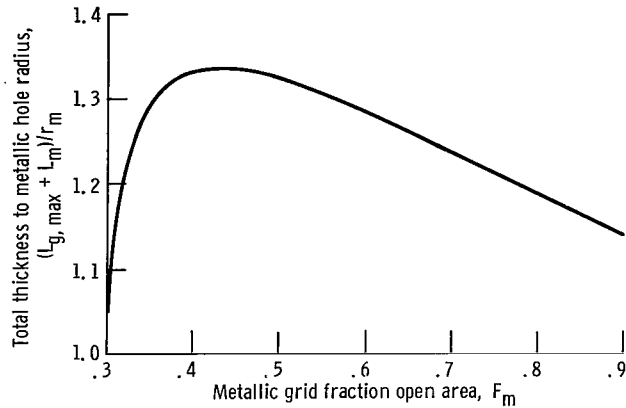


Figure 7. - Ratio of total fused-glass-composite thickness to metallic grid-hole radius as function of metallic-grid fraction open area for stability limited coatings (eq. (5)).

process which reduces the size and number of bubbles normally formed during fabrication would increase the effective breakdown strength. This is the subject of the next section of the report.

### Helium Bubble Reduction Process

When the glass particles fuse together during grid fabrication it is possible for numerous bubbles to be formed in the molten glass. These are formed because of encapsulation of the environmental atmosphere which fills the voids found between the glass particles. However, if the encapsulated gas (i. e., the environmental atmosphere) is helium, bubble collapse will occur because of the high rate of helium diffusion through glass (ref. 5).

Appendixes C and D consist of theoretical developments that show that helium bubbles can be made to collapse either by switching to a different background environmental gas during the process (appendix C) or by simply letting the molten glass remain in the helium environment (appendix D). Results from the treatment in appendixes C and D are presented next in the form of plots in figures 8 to 11.

Figures 8(a) and (b) show bubble radii as a function of diffusion time for a range of typical initial bubble radii  $r_{B,0}$  for the two environmental methods. For both cases, the smaller the initial bubble radius, the shorter the bubble collapse time. In the helium switched to a nonhelium environment case (fig. 8(a)) the helium diffuses out of the bubble due to a concentration gradient developed in the glass between the zero pressure background helium environment and the helium pressure in the bubble. For a helium only environment (fig. 8(b)) the concentration gradient is much smaller since the background en-

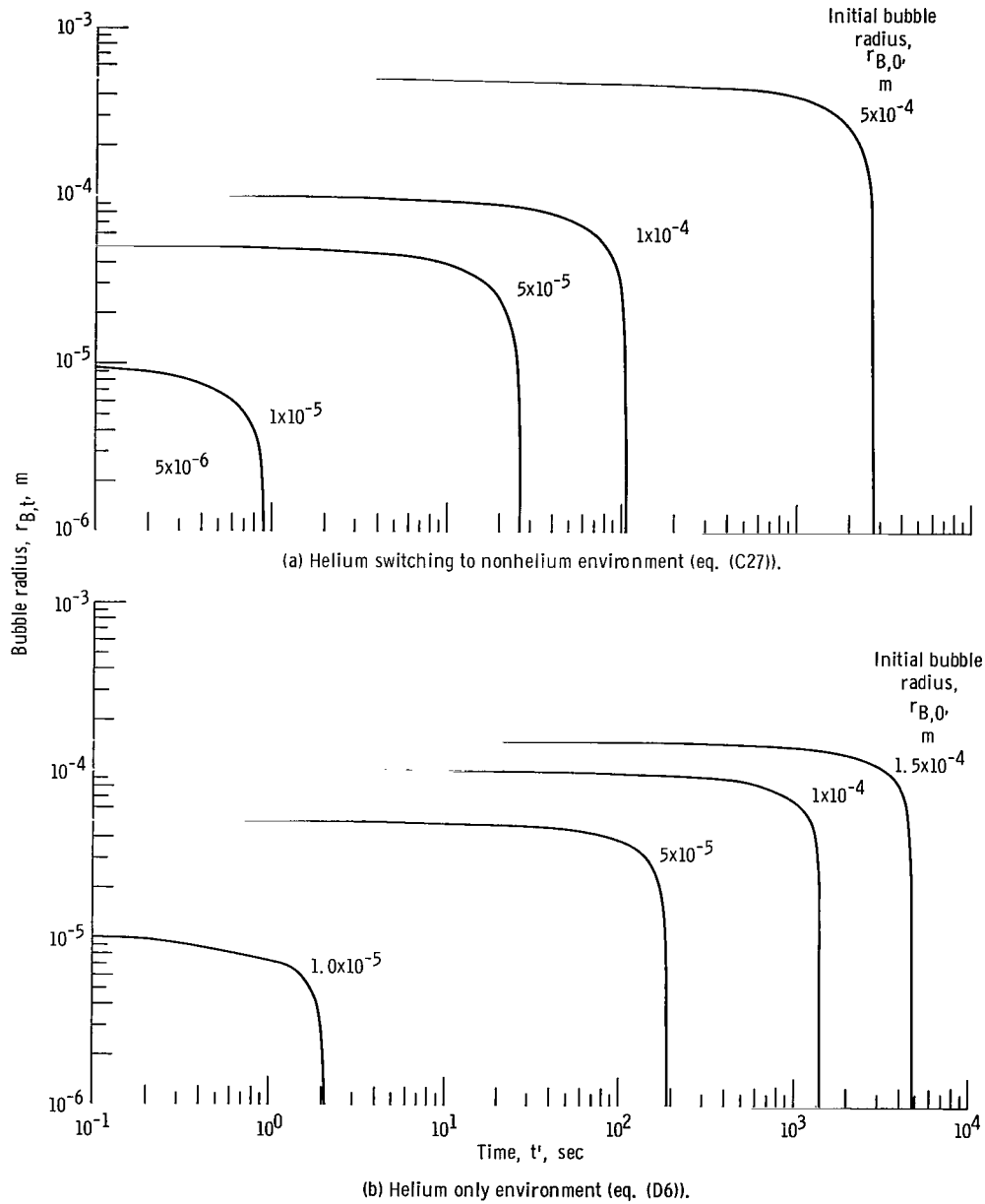


Figure 8. - Calculated bubble radius as function of time for helium bubbles in Corning glass code 7052. Bubble temperature ( $T_B = T'_B$ ), 1444 K; helium permeability coefficient at  $T_B$  or  $T'_B$ ,  $4.56 \times 10^{-11}$  square meter per second; standard pressure,  $1.0 \times 10^5$  newtons per square meter; coefficient of surface tension of Corning glass code 7052,  $2.73 \times 10^{-1}$  newton per meter.

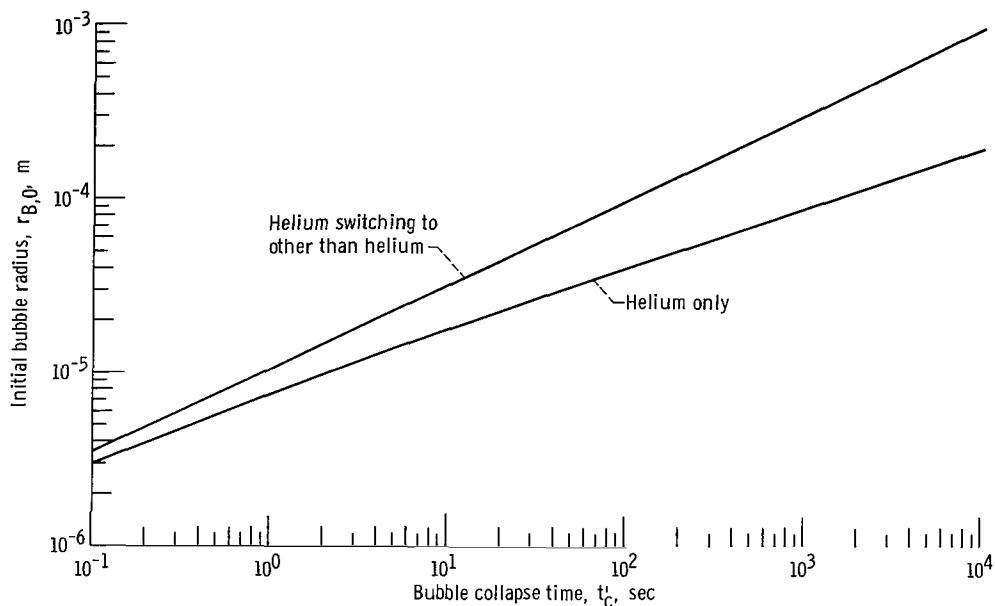


Figure 9. - Bubble collapse time as function of initial bubble radius for helium switching to nonhelium gas (eq. (C28)) and helium only (eq. (D7)).

environment is at 1 atmosphere of helium pressure. However, very small bubbles have a high helium pressure due to surface tension forces (see eq. (C22)). For these bubbles, the bubble collapse times are less dependent on the environmental gas as shown in figure 9. Figure 9 shows that the bubble collapse times for helium switched to a nonhelium environment are shorter than the collapse times for the helium only environment.

Figure 10(a) and (b) show the effects of time on bubble size distribution starting with a normal distribution. At  $t' = 0$  the mean bubble radius,  $r_{B,0}$ , was chosen to be  $1 \times 10^{-4}$  meter, the standard deviation of bubble radii was chosen to be  $1.5 \times 10^{-5}$  meter for a typical bubble distribution, and the area under the curve is equal to unity. At some later time, values for  $r_{B,t'}$  are obtained from equation (C27) for figure 10(a) and equation (D6) for figure 10(b). The area under each curves is then adjusted such that it represents the new probability of finding a bubble. This probability has been reduced (i. e., the area under the curve is less than unity) because some fraction of the bubbles have collapsed. As can be seen from figure 10(a), for helium switching to nonhelium gas, the probability distribution has changed considerably after 100 seconds. Figure 10(b) for helium only shows that after this same amount of time there is little effect on the shape of the distribution or on the magnitude of the probability. This would be expected from earlier results which indicated longer bubble collapse times for the helium only case.

For any given bubble size distribution it is also possible for bubble-to-bubble diffusion to take place in which small, high pressure bubbles diffuse helium into near-

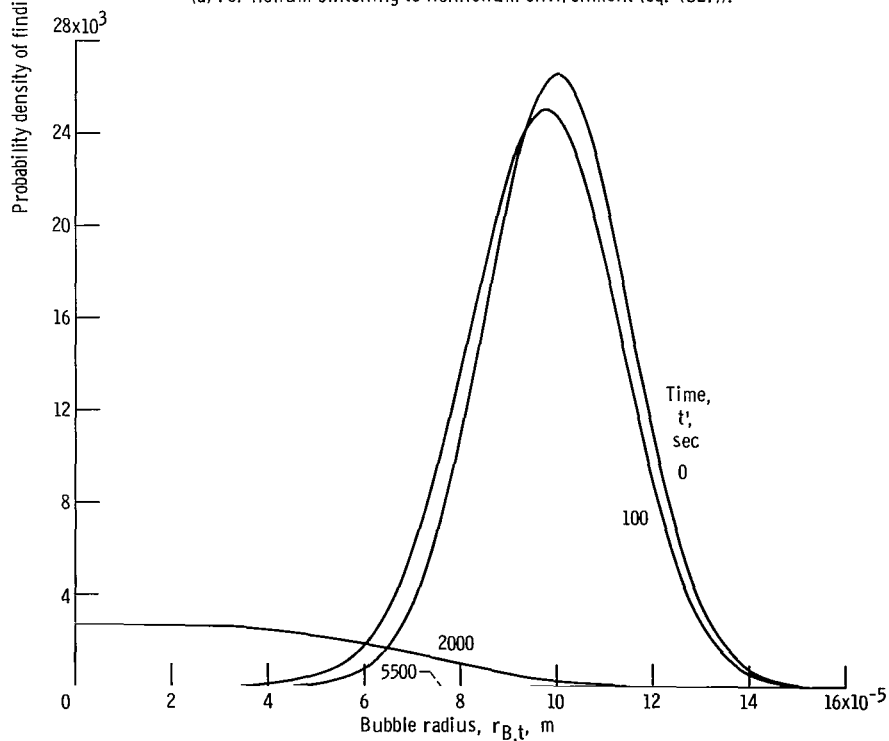
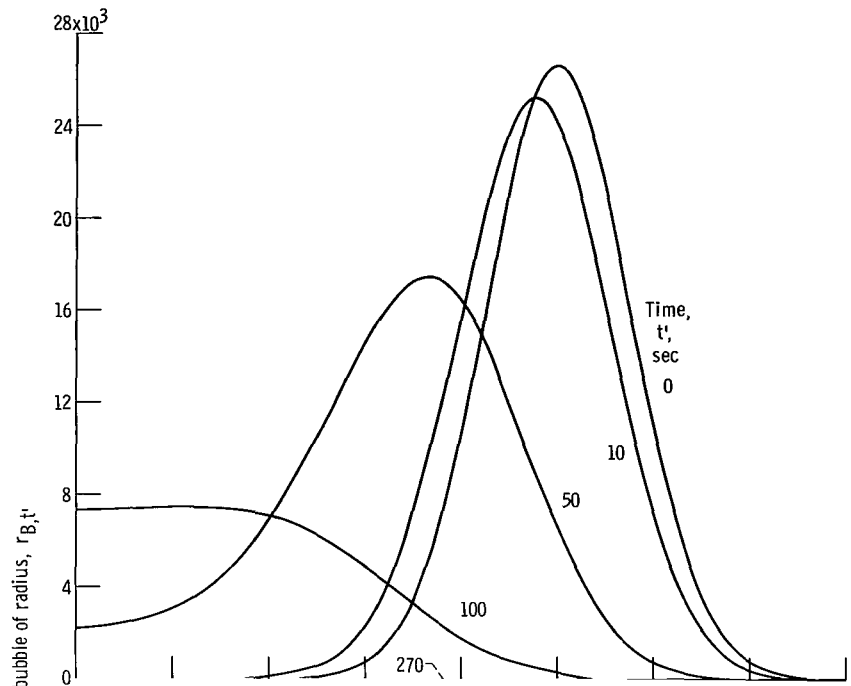


Figure 10. - Helium diffusion from initially normal distribution of bubble radii.

neighbor, large, low pressure bubbles. Analytic treatment of this complex process is beyond the scope of this report.

As a result of the preceding analysis (confirmed by experimental tests yet to be discussed) it was concluded that bubble collapse could be achieved faster by switching background gases from helium to argon at the appropriate point in time during the fabrication process.

The minimum time required at the glass fusion temperature during fabrication can be estimated from noting that the length of time required for bubble collapse is related to glass coating thickness. The thicker the coating the larger the possible initial bubble radii,  $r_{B,0}$ , and the longer the collapse time required. From experimental observations, the largest  $r_{B,0}$  values are approximately equal to one half of the fused glass thickness, that is,

$$r_{B,0} \cong \frac{L_g}{2} \quad (6)$$

Thus, if the powdered glass was slurry sprayed on the grid to a thickness which, after fusing, would amount to 0.015 centimeter, then the largest expected initial bubble radius would be 0.0075 centimeter. As can be seen from figure 9 for the helium switching to nonhelium curve, with  $r_{B,0} = 7.5 \times 10^{-5}$ , the bubble collapse time required is 57 seconds.

## Temperature Effects

All the helium diffusion time plots presented thus far have been evaluated using  $T'_B = 1444$  K as a typical fabrication temperature. It is also of interest to consider the effect on bubble collapse for fabrication at different temperatures.

The diffusion time  $t'$  is inversely proportional to the permeability coefficient  $K$ . The surface tension coefficient,  $\gamma$ , and helium solubility,  $S$ , are nearly independent of temperature but the helium diffusion coefficient,  $D$  increases with temperature as given by the expression (refs. 8 and 9)

$$D = D_0 e^{-W/(kT_B)} \quad (7)$$

where

$W$     activation energy necessary to cause diffusion

$k$     Boltzmann's constant

$D_0$  constant independent of temperature

The helium permeability coefficient,  $K$ , is given by

$$K = SD \quad (8)$$

which can be rewritten via equation (7) as,

$$K = K_0 e^{-W/(kT_B)} \quad (9)$$

where  $K_0$  is a constant independent of temperature.

Thus, the time,  $t$ , at any temperature,  $T_B$ , is found by multiplying the previously plotted time,  $t'$ , at  $T_B = T'_B = 1444$  K by the factor

$$\frac{t}{t'} = \frac{K'}{K} \quad (10)$$

or, through the use of equation (9),

$$\frac{t}{t'} = e^{-W/k \left\{ (1/T'_B) - (1/T_B) \right\}} \quad (11)$$

where  $T'_B = 1444$  K and

$$\frac{W}{k} \cong 3440 \text{ K} \quad (12)$$

for Corning glass code 7052. Figure 11 is a plot of equation (11) for converting  $t'$  to  $t$  at various temperature  $T_B$ .

Coatings thicker than prescribed by the hole wall stability limit can result in a large fraction of the holes filling in. However, the surface tension forces tending to cause hole fill-in are not very large if the coating is just slightly beyond the stability limit and can be overcome by fusing at lower temperatures. This is because of the resistance to glass flow caused by the high glass viscous drag at low temperatures. But, a low fusing temperature necessitates the use of a longer diffusion time for bubble collapse as can be seen from figure 11. The increased diffusion time allows the glass to have more time to flow which tends to detract from the advantage of using a low fusing temperature. Glass viscosity increases more rapidly with decreasing temperature than the diffusion coefficient decreases with decreasing temperature (bubble collapse time varies inversely with  $D$ ).

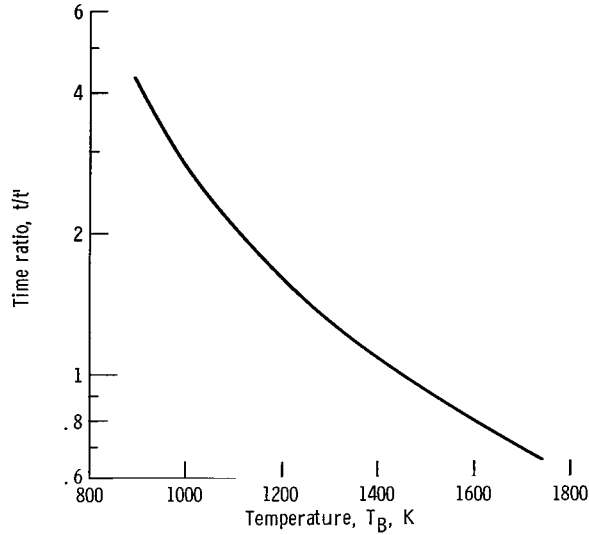


Figure 11. - Ratio of bubble collapse time at various bubble temperatures to collapse time at 1444 K as function of temperature (eq. (11)).

Thus at low temperatures bubble collapse time becomes viscosity dominated rather than diffusion dominated. For example, at 1061 K the viscosity is too high to permit any significant bubble collapse in 15 minutes of diffusion time, for a 0.15-centimeter-thick fused glass coating.

## COMPOSITE GRID FABRICATION PROCEDURE

The apparatus and procedure for fabrication of fused glass composite accelerator grids using a helium diffusion bubble reduction process is described in this section.

The choice of Corning glass code 7052 as the glass for fusing to the accelerator grid largely depended on the choice of metal for the grid and the thermal environment of the composite grid during normal operation. Molybdenum was chosen as the accelerator grid base material because of its low sputtering yield, high melting temperature, and low coefficient of thermal expansion. The glass that was chosen to fuse to the molybdenum was selected so as to have a near perfect match in thermal expansion coefficient with molybdenum, a high electrical volume resistivity, and a high viscosity at temperatures near 800 K. In addition to satisfying these requirements Corning glass code 7052 also has the desirable property of having a high helium diffusion coefficient.

The following brief description of the fabrication procedure is numbered in the order of successive design and fabrication steps.

(1) Give consideration to the geometrical relations shown in figure 7, to arrive at a suitable geometry.

(2) After the metallic grid with the desired geometry has been fabricated, sand and remove all burrs.

(3) Some means of containing the grid and supporting it by its edges is required to prevent dirt, grease, and dust from contaminating the glass prior to fusing. This seemingly trivial step is actually quite important since the quality of the glass-to-metal seal is greatly impaired by organic contamination. Also, lint and dust can cause bubbles to form in the glass during fusing.

(4) The molybdenum grid should be washed in a degreasing solvent, acetone, then distilled water to remove grease, oil, and finger print contamination. From this step on, the grid should not be touched except using rubber gloves and then only on its edges where the quality of the glass coating is least important.

(5) To produce an acceptable glass to metal seal the grid surface must be oxidized to a blue or purple color. This is achieved by inserting the grid in an electric furnace with an air environment at  $538^{\circ}$  C for 5 to 10 minutes. The grid can be periodically withdrawn and inspected to prevent excessive oxidation of the molybdenum surface. Excessive oxidation is apparent by a dull gray-white or white coating but can be washed off using distilled water. An electric furnace instead of a gas furnace is desirable so as to prevent organic combustion products from adsorbing onto the oxide layer. This can cause the layer to be reduced during the high fusing temperatures used later, thus preventing the glass from wetting the molybdenum. (The furnace should have a fume hood to prevent personnel from breathing the molybdenum oxide which appears as smoke during oxidation of the grid.)

(6) To maintain a fused glass coating on the grid upstream face and in the hole walls but not on the downstream face of the grid which must remain an electrically conductive surface, it is necessary to remove all oxide from the downstream grid face. This can be done using emery paper to sand the downstream face of the grid. Placing the grid face down on a soft plastic sheet will prevent removal of the oxide layer from the upstream face.

(7) Powdered glass can be applied to the oxide coated side of the grid by spraying a powdered glass and water slurry using a commercial paint sprayer. The slurry consists typically of equal parts by volume of the powdered Corning glass code 7052 (-325 mesh fineness) and water. Constant agitation of the suspension is necessary to insure uniform application of the coating. To apply the coating the grid should be supported by its edges so that sprayed droplets passing through the grid holes continue to travel away from it and do not collect on the downstream grid face. Waiting for the water to evaporate between each coating application prevents filling in of the holes. Several thin fused coatings are better for preventing the occurrence of large bubbles than a single thick fused glass coat-

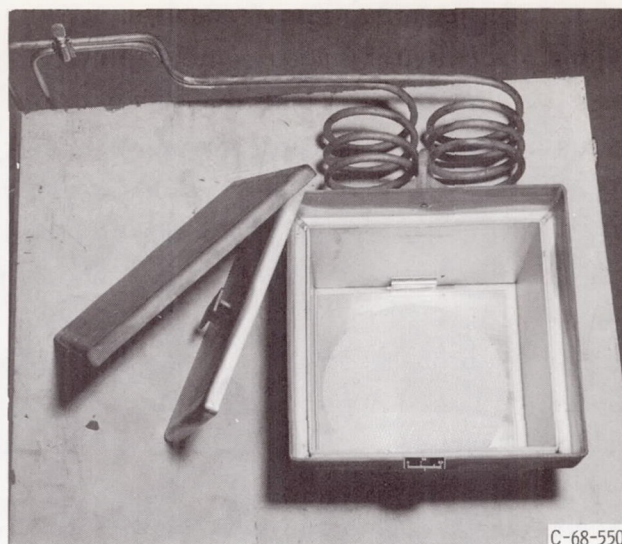


Figure 12. - Grid (15-cm diam) in the box used for environmental control during fusing.

ing. A typical fusing operation results in 0.015-centimeter-thick fused glass coating for a metal grid of 50 percent open area, 0.191-centimeter hole diameter, and 0.038-centimeter-thick molybdenum.

(8) After the slurry has dried the grid is placed in an environment control box. A box of this type (pictured in fig. 12) is made of a metal having the qualities of resisting oxidation and high strength at high temperatures (Inconel 600 and Hastelloy X are suitable materials). The box should have two lids and two chambers each with its own gas feed tube. The glass coated grid to be fused is set in the innermost chamber. The double chamber box minimizes the amount of back diffusion of oxygen into the inner chamber which would oxidize the grid. A tantalum wire mesh getter is placed over the inlet to the innermost chamber to help remove any oxygen which may feed into this chamber and to indicate if there are any leaks present in the inert gas feed system. The grid can be heated with the coated side up and either elevated by its rim from the box bottom or laid flat on a polished clean oxidation resistant tray. The glass will not stick to a smooth clean tray if the glass has a much lower coefficient of thermal expansion.

(9) After the grid is placed in the environment control box with its lids on, the box is purged with helium for at least one-half hour at room temperature to ensure all other gases have been flushed out. The gas flow rate is typically set at  $6 \times 10^{-4}$  cubic meter per second per meter of box trough circumference.

(10) While maintaining helium purging, the box with the grid is inserted in an oven at  $538^{\circ}\text{C}$  for 1/2 hour to bake any organic material out of the powdered glass while still not fusing the glass particles together. This step helps insure that when the high temperature encapsulation of the environmental gas occurs, no other gases are present due to decom-

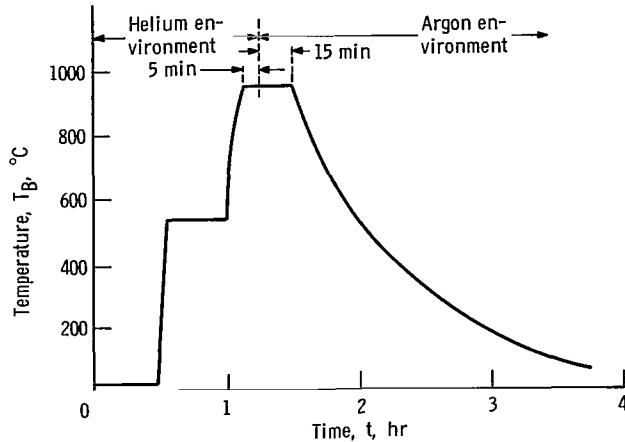


Figure 13. - Temperature-time-environment sequence for fusing powdered glass coatings on composite accelerator grid.

posing organic matter, water vapor or other adsorbed or absorbed gases.

(11) While still maintaining helium purging, the box with the grid is inserted in an oven preheated to the desired fusing temperature for the glass coating. The amount of time required will depend on the heatup time for the environment control box and the viscosity of the glass at the particular fusing temperature chosen. Typically, 20 to 30 minutes is sufficient time for a room temperature environment control box to heat up in a 760 C oven and completely fuse the Corning glass code 7052 particles together.

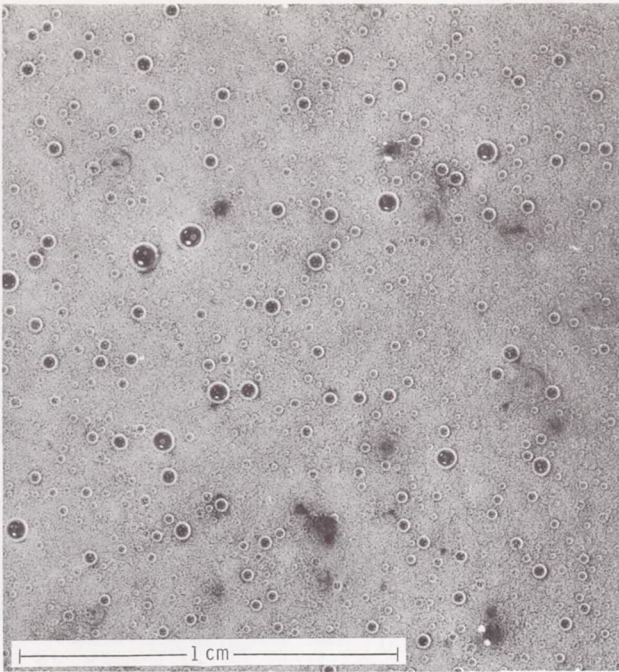
(12) After encapsulation is complete change the purging gas to argon and allow 15 minutes for helium diffusion out of the bubbles. Remove the inert environment control box from the oven while continuing the argon purging and allow to air cool to room temperature. This time-temperature-environment sequence is shown in figure 13.

(13) For the second and additional coatings start at step 6 and repeat the coating and fusing scheme, until the desired glass coating thickness is achieved.

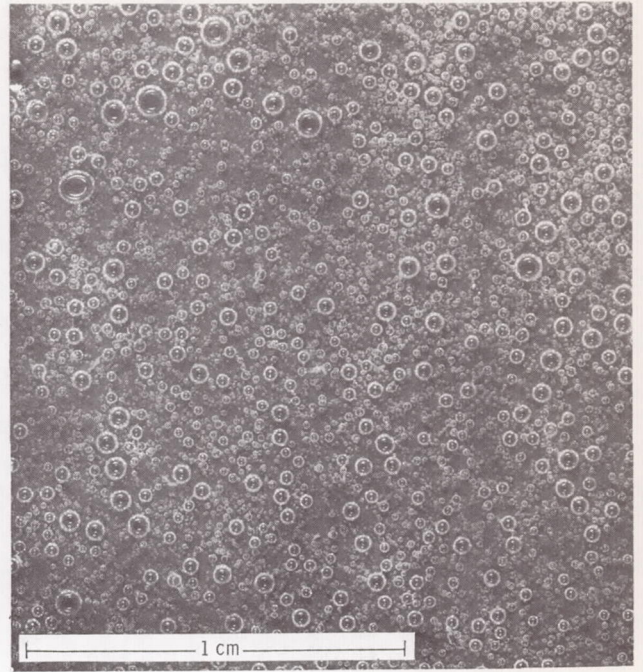
(14) Prior to grid operation in a thruster, the grid's downstream face should again be sanded to expose an entirely electrically conducting surface.

## EXPERIMENTAL TESTS AND RESULTS

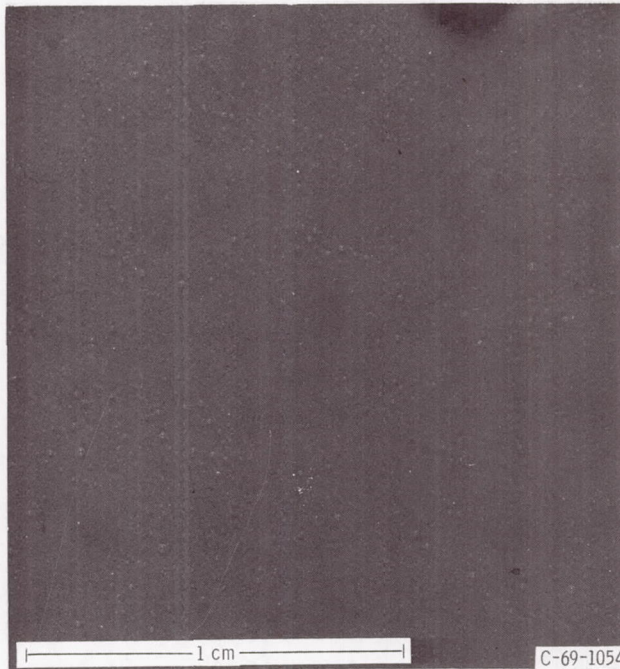
The effectiveness of the helium-argon diffusion process for eliminating bubbles has been tested and compared with other processes for which the time-temperature history was the same. Figure 14 shows coatings made using various background gases. Figure 14(a) is for an argon environment only, figure 14(b) is for a helium environment only, and figure 14(c) is for a helium-followed-by-argon environment. Figure 14(a) shows numerous large and small bubbles present indicating that negligible bubble collapse has oc-



(a) Coating fused in argon only environment resulting in many large and small bubbles.



(b) Coating fused in helium only environment resulting in numerous big bubbles but few small bubbles.



(c) Coating fused using the helium-switched-to-argon environment. Dark appearance is because glass is nearly bubble free.

Figure 14. - Fused Corning glass code 7052 coatings on molybdenum made with various background gases. Coating thickness, 0.2 millimeter; fusing temperature, 1444 K.

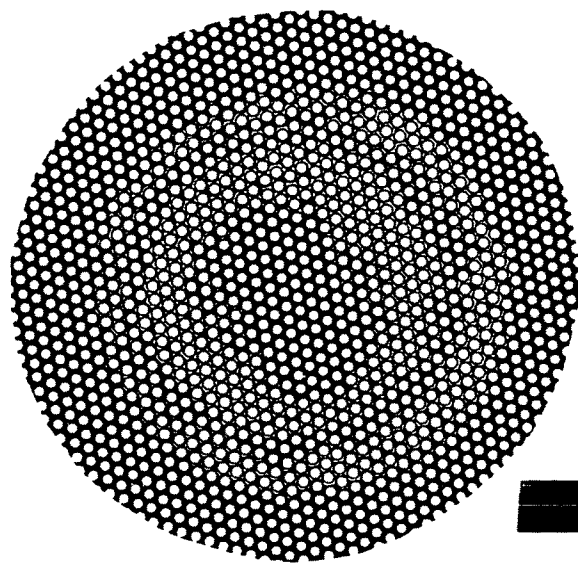
curred during fabrication. Figure 14(b) shows many large bubbles remaining since only the small radius bubbles have had time to collapse. This is because only the small radius bubbles have pressures large enough to cause significant helium diffusion into the helium environment. Figure 14(c) appears much darker than the previous photos because there are very few bubbles present and only the dark oxide coated glass-molybdenum interface is observed. This absence of bubbles tends to agree with the theoretical predictions shown in figure 10(a). In the fabrication of the sample shown in figure 14(c) 900 seconds was allotted for bubble diffusion. And as can be seen from figure 10(a) virtually all bubbles should be collapsed after 270 seconds.

Electrical breakdown measurements were made to compare typical breakdown strengths of glass coated on molybdenum using the argon only environment and the helium followed by argon environment. The tests were performed using an unperforated parallel plate geometry. Electrodes were placed on each side of the sample which was then immersed in oil to prevent atmospheric breakdown. For glass coatings of 0.035-centimeter average thickness, the average electrical breakdown strength was  $8.75 \times 10^7$  volts per meter for the nearly bubble free glass made using the helium-argon process, more than a factor of 8 improvement over the value obtained with the argon-only process.

As a result of confirmation of the fabrication process with the previously described tests, a 5-centimeter grid was fabricated for testing on a thruster. The thruster is described in detail in reference 4. The grid was fabricated using the helium-argon process. The temperatures chosen for glass fusing for this grid were 1444, 1277, and 1166 K for the first, second, and third coating, respectively.

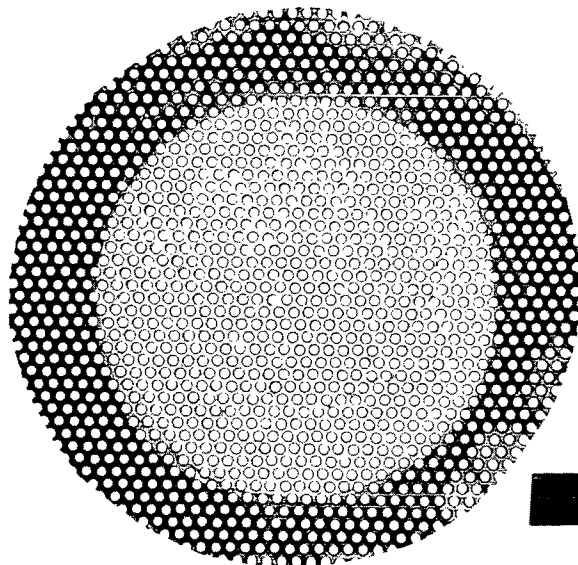
Figures 15(a) and (b) are photographs of upstream (coated) face and downstream (uncoated) face, respectively, of the grid after more than 200 hours operation without failure. The molybdenum portion of the grid is 0.038-centimeter thick with 50 percent open area having 0.91-centimeter-diameter holes. The maximum glass coating thickness  $L_{g, \max}$  is 0.0465 centimeter. Figure 7 indicates that this thickness is 53 percent of the maximum allowable glass coating thickness as given by the hole wall stability limit. The operating voltages for this grid were  $V_1 = 400$  volts and  $V_a = -220$  volts (i. e.,  $\Phi_g = 620$  volts) for a 0.032-ampere mercury-ion beam. For stable operation it was found necessary to use a neutralizer emitting at least one-third of the beam current.

A glass coated grid has also been fabricated and tested on a 30-centimeter-diameter Kaufman thruster. Figure 16 is a photograph of the grid mounted on the thruster. The molybdenum portion of the grid is of the same geometry as the 5-centimeter grid shown in figure 15. Use of prepunched molybdenum saves considerable fabrication time by eliminating the need of drilling the more than 12 000 holes in the grid. The fusing and helium diffusion temperatures used for the glass coating layers were 1283, 1172, 1116, and 1061 K, for the first to fourth coating, respectively. The first three glass coatings were nearly bubble free but the last coating was not because, as discussed earlier, the



C-67-3503

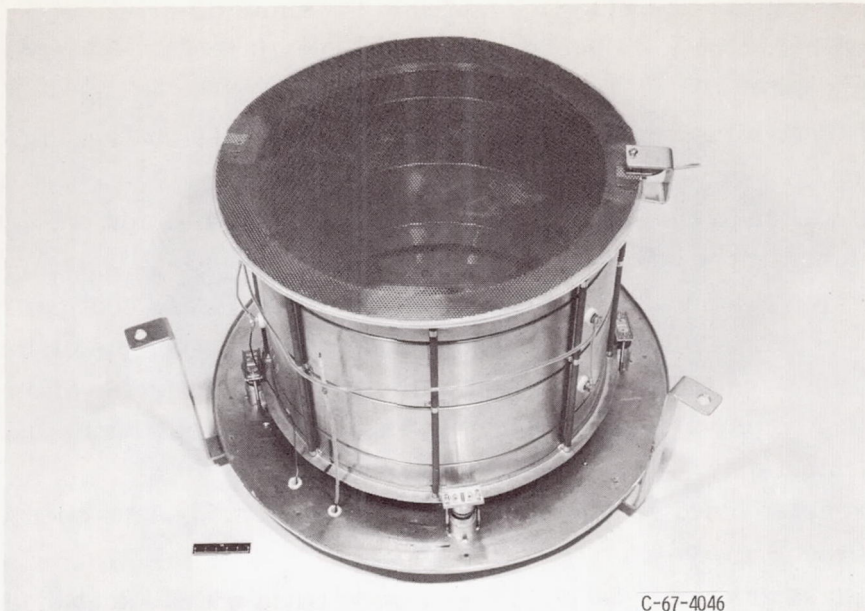
(a) Upstream face coated with Corning glass code 7052.



C-67-3502

(b) Downstream face with central region appearing shiny due to sputtering.

Figure 15. - Fused glass composite accelerator grid for a 5-centimeter-diameter Kaufman mercury-ion thruster.



C-67-4046

Figure 16. - Fused glass composite accelerator grid mounted on 30-centimeter Kaufman mercury-ion thruster.

glass viscosity was too high. The maximum coating thickness for this grid is 0.0508 centimeter which is 58 percent of stability limited glass thickness.

Some tests to ascertain the structural integrity of glass coated grids have been conducted. Flat grids for 5-centimeter thrusters have withstood shake tests exciting the drum mode of oscillation at levels of 30 g's of random noise (20 to 20 000 Hz) and 40'g of sinusoidal oscillation (39 to 3000 Hz). In these tests the fused glass composite grid was clamped by its edges beyond a 6.7-centimeter-diameter circle. Flight-type, fused-glass composite accelerator grids with larger diameter-to-thickness ratios may require that the grids be dish shaped and possibly have stiffening ribs across the diameter to prevent drum modes of oscillation which could cause the glass to crack off. A dished fused glass composite grid of this type with an integral electrically isolated retaining assembly for a 15-centimeter-diameter thruster is described in reference 10.

## CONCLUDING REMARKS

A method has been developed to produce fused glass coatings suitable for composite accelerator grids for electron-bombardment ion thrusters.

The following conclusions can be drawn from this study:

1. Fabrication of nearly bubble free glass coatings is possible using conveniently available processes, temperatures, and diffusing times. The process involves the

switching from a helium environment to an argon environment when the glass is at temperatures near 1444 K and allowing 15 minutes for helium diffusion.

2. Electrical breakdown of the glass coating occurs if there are large bubbles and/or numerous small bubbles in the glass.

3. A hole wall stability limit exists which limits the glass coating thickness for a given grid geometry.

4. A theoretical analysis that was made gives useful results for predicting minimum glass coating temperatures and times for bubble collapse.

5. The effective electrical breakdown strength of fused glass coatings on unperforated plates made by the helium diffusion process is  $8.75 \times 10^7$  volts per meter for coatings of approximately 0.035-centimeter thickness. This represents a factor of more than 8 improvement in effective electrical breakdown strength over fused glass coatings made in an argon environment only.

6. Small diameter fused glass composite accelerator grids have operated successfully for over 200 hours.

7. A fused glass grid for a 5-centimeter thruster has withstood shake tests exciting the drum mode of oscillation at levels of 30 g's of random noise (20 to 2000 Hz) and 40 g's of sinusoidal oscillation (39 to 3000 Hz). However, grids with larger diameter-to-thickness ratios may require additional structural support.

Lewis Research Center,  
National Aeronautics and Space Administration,  
Cleveland, Ohio, March 18, 1969,  
120-26-02-06-22.

# APPENDIX A

## SYMBOLS

c	constant, $\text{N}/\text{m}^2$	r	radius, m
D	diffusion coefficient, $\text{m}^2/\text{sec}$	$r_{B,t}$	bubble radius at time t, m
$D_o$	constant independent of temperature, $\text{m}^2/\text{sec}$	$r_{B,o}$	bubble radius at time $t = 0$ , m
$d_m$	distance from metallic surface to bubble center, m	S	solubility, dimensionless
$d_s$	distance from glass surface to bubble center, m	T	temperature, K
E	electric field magnitude, $\text{V}/\text{m}$	$T_o$	standard temperature, 273.15 K ( $0^\circ \text{C}$ )
F	fraction open area, dimensionless	$T_B$	bubble temperature, K
K	helium permeability coefficient at temperature $T_B$ or $T'_B$ , $\text{m}^2/\text{sec}$	$T'_B$	fixed bubble temperature of 1444 K ( $1171^\circ \text{C}$ )
$K_o$	constant independent of temperature, $\text{m}^2/\text{sec}$	t	time, sec
k	Boltzmann's constant, $1.38054 \times 10^{-23}$ , J/K	$t'$	time for $T_B = T'_B$ , sec
L	thickness, m	$V_B$	volume of bubble, $\text{m}^3$
M	mass per mole of helium, $4.0026 \times 10^{-3}$ kg/mole	$V_a$	accelerator voltage, V
$m_B$	mass of helium within a bubble, kg	$V_I$	net accelerating voltage, V
P	pressure, $\text{N}/\text{m}^2$	$V_o$	normal volume of a perfect gas, $\text{m}^3/\text{mole}$
$P_o$	standard pressure, $1.013 \times 10^5$ $\text{N}/\text{m}^2$	W	activation energy necessary to cause helium diffusion in Corning glass code 7052, J
R	radial distance measured parallel to the glass surface from the axis of symmetry line drawn perpendicular to the glass surface through the bubble center (see fig. 19), m	w	minimum metallic web distance for a hexagonal array of hole, m
		x, y, z	rectangular Cartesian coordinates, m
		$\gamma$	coefficient of surface tension Corning glass code 7052, $\text{N}/\text{m}$
		$\kappa$	dielectric constant of Corning glass code 7052, dimensionless
		$\rho$	helium mass density, $\text{kg}/\text{m}^3$

$\Phi_g$  electrical potential applied across  
glass coating, V

Subscripts:

B bubble  
b breakdown  
c collapse

g glass  
h hole  
m metal  
max maximum  
s glass surface  
t time  
t' time for  $T_B = T'_B$

## APPENDIX B

### FUSED GLASS HOLE WALL STABILITY

In this section we consider the effect of surface tension forces on the stability of a glass coating applied to an irregular surface. Relations are developed that permit prediction of the maximum coating thickness on a grid without the occurrence of hole fill in. During the fusing process for a typical accelerator grid the liquid glass surface tension forces dominate over other forces such as gravitational body forces on the glass. Thus the glass will always assume a geometry that possesses a minimum surface tension energy. In order that the problem can be treated analytically it is convenient to assume that the liquid surface is a doubly curved surface of radii of curvature  $r_1$  and  $r_2$  as shown

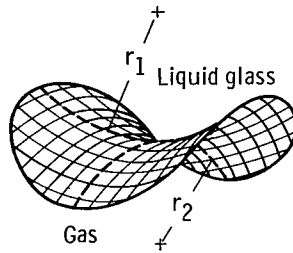


Figure 17. - Doubly curved glass-gas interface.

in figure 17. The pressure difference  $\Delta P$  (resulting from the surface tension forces) across an element of the surface is given by reference 11.

$$\Delta P = \gamma \left( \frac{1}{r_1} - \frac{1}{r_2} \right) \quad (\text{B1})$$

where  $\gamma$  is the surface tension coefficient of the liquid glass-gas interface. For the case of a hole in the glass surface (as shown in fig. 5) the pressure difference tending to force the liquid glass surface away from the center of a hole becomes

$$\Delta P = \gamma \left( \frac{1}{r_{g, \max}} - \frac{1}{r_h} \right) \quad (\text{B2})$$

where  $\Delta P$  is the pressure acting on surface elements which lie on the glass surface

circles of radii,  $r_h$ , and  $r_{g, \max}$ . The radius  $r_{g, \max}$  is postulated to be the largest radius which can be drawn in the plane of the grid from the metallic web intersection to the nearest glass hole wall surface (see fig. 5(a)). If the glass coating is so thick that  $r_{g, \max} > r_h$  then the surface pressure will force the hole walls to collapse and fill in the hole with glass. The hole wall will be stable if  $r_h > r_{g, \max}$  everywhere around the hole.

To determine if  $r_{g, \max}$  as defined above is the appropriate characteristic radius to be compared with  $r_h$  a statistical analysis was performed on a grid coated to such an extent that 127 of its 2433 holes were filled in due to surface tension forces. Diameters of all the holes were measured using an optical comparator and the data was plotted on probability scale graph paper as shown in figure 18. A value of  $r_{g, \max} = 0.294$  millimeter was predicted by measurements made on the uncoated grid and using the following geometrical relation

$$r_{g, \max} = \frac{2r_m + w}{2\sqrt{3}} \quad (B3)$$

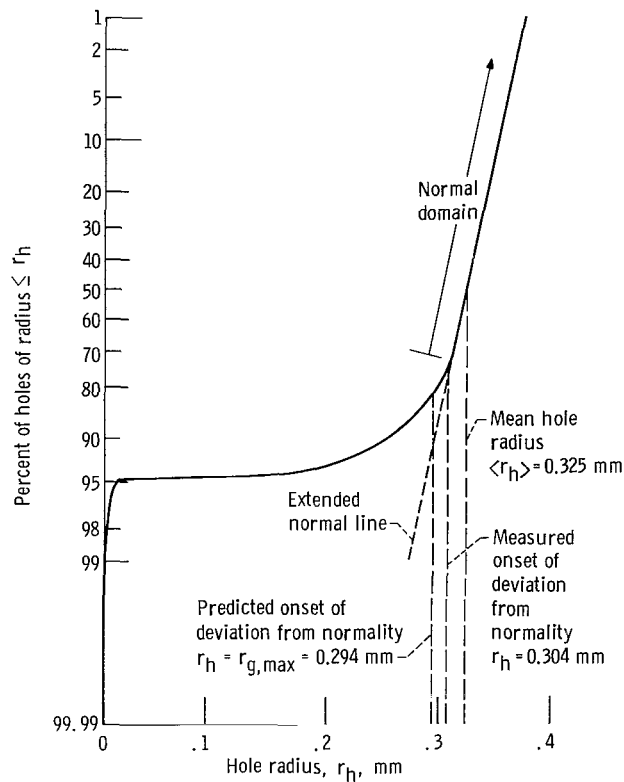


Figure 18. - Hole radius distribution.

where  $w$  is the minimum width metallic web between adjacent holes (see fig. 5(a)). For hole radii greater than the glass radii  $r_{g, \max}$  the distribution of hole radii should be a normal or Gaussian distribution.

The data in figure 18 indicates that this is the case. A significant deviation from this normal distribution would be expected for  $r_h < r_{g, \max}$  since in this case hole wall instability occurs and these holes would fill in.

As can be seen from figure 18 the experimentally measured point of onset of deviation from normality occurs very close (within experimental error) to the predicted value of  $r_{g, \max} = r_h$ .

Using  $r_{g, \max}$  as given by equation (B3), a glass thickness  $L_g$ , a metallic grid thickness,  $L_m$ , and metallic grid fraction open area  $F_m$ , a relation can be developed to determine the maximum stable coating thickness  $L_{g, \max}$  as a function of  $L_m$ ,  $r_m$ , and  $F_m$ . As can be easily identified from figure 5(b)

$$L_g = r_{g, \max} + \sqrt{r_{g, \max}^2 - (r_h + r_{g, \max} - r_m)^2} - L_m \quad (B4)$$

From figure 5(a) it can be shown that

$$F_m = \frac{2\pi}{3\sqrt{3}} \left( \frac{r_m}{r_h + r_{g, \max}} \right)^2 \quad (B5)$$

When the glass coating is at the limit of stability then  $r_h = r_{g, \max}$  and equation (B5) becomes,

$$r_{g, \max} = r_m \sqrt{\frac{\pi}{6\sqrt{3} F_m}} \quad (B6)$$

Combining equations (B4) to (B6) to obtain  $L_{g, \max}$  yields

$$L_{g, \max} = r_m \sqrt{\frac{\pi}{6\sqrt{3} F_m}} \left[ 1 + \sqrt{1 - \left( 2 - \sqrt{\frac{6\sqrt{3} F_m}{\pi}} \right)^2} \right] - L_m \quad (B7)$$

where  $F_m > \pi/6 \sqrt{3} \cong 0.3027$ . Also to prevent exposure of the plasma to the upstream hole wall edge (for holes such as in fig. 5(b)) the glass coating radius  $r_{g, \max}$  must be large enough to extend beyond this edge. Direct impingement on the grid would occur if the glass coating was so thin that the upstream hole wall edge was exposed to the discharge plasma. To prevent this condition

$$r_{g, \max} > \sqrt{\left[ L_m - \sqrt{r_{g, \max}^2 - (r_h + r_{g, \max} - r_m)^2} \right]^2 + (r_h + r_{g, \max} - r_m)^2} \quad (\text{B8})$$

which reduces to

$$L_m < 2 \sqrt{r_{g, \max}^2 - (r_h + r_{g, \max} - r_m)^2} \quad (\text{B9})$$

Choosing the largest value of the right side of equation (B9) as dictated by the stability limit using equations (B5) and (B6) gives

$$L_m < 2r_m \sqrt{\frac{\pi}{6 \sqrt{3} F_m} \left[ 1 - \left( 2 - \sqrt{\frac{6 \sqrt{3} F_m}{\pi}} \right)^2 \right]} \quad (\text{B10})$$

This ensures that the upstream edge of the hole walls will be covered with glass. However, equation (B10) is not valid if the metal grid holes are chambered, tapered, or of any cross section other than rectangular as shown in figure 5(b).

In summary, in the interest of minimizing electrical breakdown of the glass coating on a fused glass composite accelerator grid, the coating thickness can be made a maximum value given by  $L_{g, \max}$  (eq. (B7)). At this glass thickness and larger thicknesses the glass hole walls are unstable due to surface tension forces and many will collapse during the fusing process. It may be possible to fabricate a grid having an  $L_g > L_{g, \max}$ , however, since hole wall collapse takes place in a finite amount of time which depends on the viscosity of the glass. Thus by a proper fusing technique it may be possible to manufacture a grid having a thicker coating without holes filling in. But the probability of having some holes fill in increases greatly with  $L_g$  once  $L_g > L_{g, \max}$ .

## APPENDIX C

### HELIUM DIFFUSION THEORY FOR HELIUM BUBBLES IN GLASS WITH DIFFUSION TO NONHELIUM ENVIRONMENTAL GAS

The process for reducing the number and size of bubbles in the glass consists of first fusing the glass powder in a helium atmosphere. When all the glass has melted, encapsulating helium gas during fusing, the environmental gas is switched to argon or some gas other than helium. While the glass is very hot and molten the helium diffuses out of the bubbles, through the glass, and into the argon environment. As a result, the bubbles reduce in size due to the helium escaping out of each bubble.

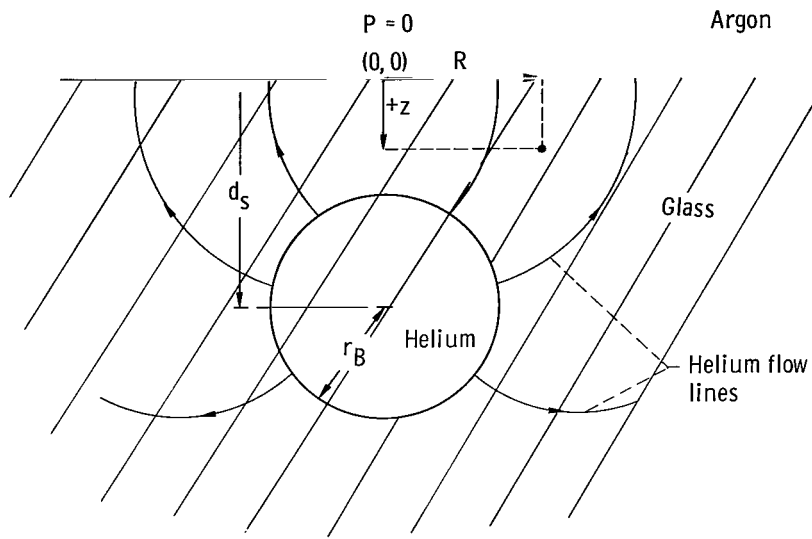
In this section we develop theoretical relations useful for predicting the bubble collapse time as a function of initial bubble radius. The following pertinent assumptions are made for a single bubble theory for this process (see fig. 19(a)).

- (1) Before time  $t = 0$  the fusing environment is 100 percent helium gas at atmospheric pressure  $P_0$  and temperature  $T_B$ .
- (2) At time  $t \geq 0$  all bubbles in the glass contain helium gas and the background environment gas is argon (or any gas other than helium).
- (3) At time  $t > 0$  the only diffusion process is helium diffusion which is caused by helium concentration gradients in the glass.
- (4) Molten glass surface tension forces act to increase the bubble pressure.
- (5) The bubble reduces in diameter at a rate fast enough to always be in equilibrium (i. e., it will not change in diameter with time if the diffusion is instantaneously stopped) but slow enough so that the diffusion can be treated as a steady-state process where the slowly changing bubble diameter does not greatly affect the diffusion process.
- (6) The glass viscosity is high enough so that bubbles do not float to the surface but low enough to satisfy assumption 5.
- (7) Helium behaves such that it satisfies the ideal gas law.
- (8) The pressure in the bubble is independent of position within the bubble for all time.
- (9) The analysis is for  $d_s/r_B \gg 1$  (see fig. 19(a)); that is, the bubble depth  $d_s$  is very much greater than the bubble radius  $r_B$ .

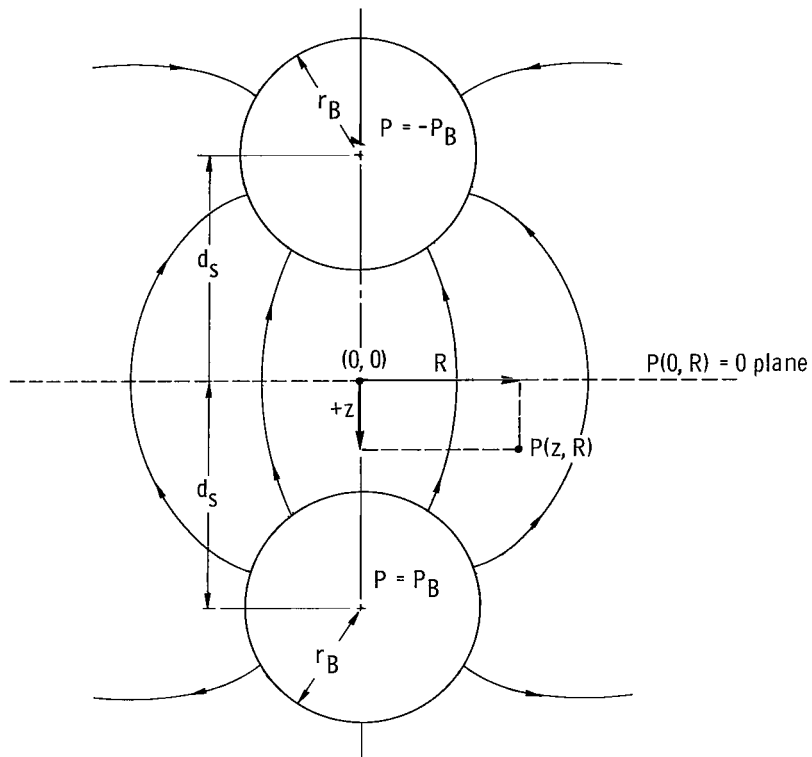
The diffusion equation is given in reference 11 as

$$D\nabla^2 \rho = \frac{\partial \rho}{\partial t} \quad (C1)$$

where  $D$  is the diffusion coefficient for helium through the particular glass used at some temperature,  $\rho$  is the helium mass density, and  $t$  is time.



(a) Physical case where  $P$  is the pressure or equivalent mass density.



(b) Potential analog where  $P$  is the electrical potential.

Figure 19. - Model for helium diffusion out of bubble.

Under the assumption of steady state, equation (C1) can be written as

$$\nabla^2 \rho = 0 \quad (C2)$$

Also  $\rho$  is proportional to pressure  $P$  since the temperature is constant throughout, or, in general

$$\rho = \frac{MPT_o}{V_o P_o T} \quad (C3)$$

where the subscripts refer to standard conditions. Substituting into equation (C2),

$$\nabla^2 \left( \frac{MPT_o}{V_o P_o T} \right) = 0 \quad (C4)$$

After removing the constants, equation (C4) reduces to

$$\nabla^2 P = 0 \quad (C5)$$

The problem is to determine  $P = P(x, y, z)$  for a bubble with an internal helium pressure  $P_B$  and a glass-argon interface at  $P = 0$  (fig. 19(a)) with the solution satisfying Laplace's equation. To arrive at a solution by analogy,  $P$  can be considered to be represented by an electrical potential. The use of an equal and opposite image potential  $-P$  will result in the same solution as for the ground plane  $P = 0$  geometry (see fig. 19(b)).

Equating pressure to electrical potential, the pressure in the glass as a function of  $Z$  and  $R$  for  $Z > 0$  and  $d_s/r_B \gg 1$  is given by

$$P(z, R) = \frac{cr_B}{\sqrt{R^2 + (d_s - z)^2}} - \frac{cr_B}{\sqrt{R^2 + (d_s + z)^2}} \quad (C6)$$

where  $c = \text{constant}$  such that

$$P(z, R) = P_B \quad (C7)$$

for

$$\sqrt{R^2 + (d_s - z)^2} = r_B \quad (C8)$$

Thus

$$z = d_s \pm \sqrt{r_B^2 - R^2} \quad (C9)$$

and equation (C5) yields

$$P_B = c - \frac{cr_B}{\sqrt{R^2 + \left(2d_s \pm \sqrt{r_B^2 - R^2}\right)^2}} \quad (C10)$$

Neglecting small terms since  $r_B/d_s \ll 1$  yields  $c = P_B$  thus

$$P(z, R) = P_B r_B \left[ \frac{1}{\sqrt{R^2 + (d_s - z)^2}} - \frac{1}{\sqrt{R^2 + (d_s + z)^2}} \right] \quad (C11)$$

To find a relation between bubble radius and time, the steady-state rate of change of helium mass in the bubble,  $\dot{m}_B$ , must be determined. The helium mass flow rate through the flat glass surface can be written as

$$\dot{m}_B = -K \int_{R=0}^{\infty} 2\pi R \left( \frac{\partial \rho}{\partial z} \right)_{z=0} dR \quad (C12)$$

where  $K$  is the helium permeability constant which is a product of the diffusion coefficient and the solubility of the glass for helium. Through the use of equation (C3) where  $T = T_B$ , equation (C12) becomes

$$\dot{m}_B = -K \frac{MT_o K}{V_o P_o T} \int_{R=0}^{\infty} 2\pi R \left( \frac{\partial P}{\partial z} \right)_{z=0} dR \quad (C13)$$

Partial differentiation of equation (C11) yields

$$\left(\frac{\partial P}{\partial z}\right)_{z=0} = \frac{2P_B r_B d_s}{(R^2 + d_s^2)^{3/2}} \quad (C14)$$

Equation (C13) thus can be rewritten as

$$\dot{m}_B = -\frac{4\pi K M T_o P_B r_B d_s}{V_o P_o T_B} \int_{R=0}^{\infty} \frac{R dR}{(R^2 + d_s^2)^{3/2}} \quad (C15)$$

Carrying out the integration of equation (C15) gives

$$\dot{m}_B = -\frac{4\pi K M P_B T_o r_B}{V_o P_o T_B} \quad (C16)$$

Thus the helium mass flow rate out of the bubble is independent of bubble depth,  $d_s$ , for deep small bubbles ( $d_s/r_B \gg 1$ ). Now that  $\dot{m}_B$  is determined it can be expressed in terms of rate of change in bubble volume  $V_B$ , and bubble pressure  $P_B$ . The mass of helium within the bubble is simply

$$m_B = \rho_B V_B \quad (C17)$$

Using equation (C3) with  $\rho = \rho_B$ ,  $T = T_B$  and  $P = P_B$  results in

$$m_B = \frac{M V_B P_B T_o}{V_o P_o T_B} \quad (C18)$$

where  $M$ ,  $V_o$ ,  $T_o$ ,  $T_B$ ,  $P_o$  are all constants. Thus

$$\dot{m}_B = \frac{M T_o}{V_o P_o T_B} \left( V_B \frac{dP_B}{dt} + P_B \frac{dV_B}{dt} \right) \quad (C19)$$

Also

$$V_B = \frac{4}{3} \pi r_B^3 \quad (C20)$$

or

$$\frac{dV_B}{dt} = 4\pi r_B^2 \frac{dr_B}{dt} \quad (C21)$$

The bubble pressure is equal to the atmospheric pressure plus the pressure due to surface tension of the glass. Thus

$$P_B = P_o + \frac{2\gamma}{r_B} \quad (C22)$$

Differentiating (C22) yields,

$$\frac{dP_B}{dt} = -\frac{2\gamma}{r_B^2} \frac{dr_B}{dt} \quad (C23)$$

Rewriting equation (C19) using equations (C20) to (C23) results in

$$\dot{m}_B = \frac{MT_o}{V_o P_o T_B} \left[ \left( \frac{4\pi r_B^3}{3} \right) \left( -\frac{2\gamma}{r_B^2} \frac{dr_B}{dt} \right) + \left( P_o + \frac{2\gamma}{r_B} \right) \left( 4\pi r_B^2 \frac{dr_B}{dt} \right) \right] \quad (C24)$$

Equation (C16) for  $\dot{m}_B$  can be also rewritten using equation (C22) yielding

$$\dot{m}_B = -\frac{4\pi KMT_o}{V_o P_o T_B} \left( P_o + \frac{2\gamma}{r_B} \right) r_B \quad (C25)$$

Setting equation (C25) equal to equation (C24) and integrating from  $r_B = r_{B,o}$  at  $t = 0$  to  $r_B = r_{B,t}$  at  $t = t$  yields

$$\int_{r_B=r_{B,o}}^{r_{B,t}} \left[ r_B - \frac{2\gamma r_B}{3(P_o r_B + 2\gamma)} \right] dr_B = -K \int_{t=0}^t dt \quad (C26)$$

Carrying out the integration and evaluation at the limits results in

$$t = \frac{1}{2K} \left\{ r_{B,0}^2 - r_{B,t}^2 - \frac{4\gamma}{3P_0} \left[ r_{B,0} - r_{B,t} - \frac{2\gamma}{P_0} \ln \left( \frac{2\gamma + P_0 r_{B,0}}{2\gamma + P_0 r_{B,t}} \right) \right] \right\} \quad (C27)$$

The time for bubbles of initial radius  $r_{B,0}$  to collapse completely to  $r_B = 0$  at  $t = t_c$  is thus given by

$$t_c = \frac{1}{2K} \left\{ r_{B,0}^2 - \frac{4\gamma}{3P_0} \left[ r_{B,0} - \frac{2\gamma}{P_0} \ln \left( 1 + \frac{P_0 r_{B,0}}{2\gamma} \right) \right] \right\} \quad (C28)$$

## APPENDIX D

### HELIUM DIFFUSION THEORY FOR HELIUM BUBBLES IN GLASS WHILE MAINTAINED IN A HELIUM ENVIRONMENT

The calculational procedure for the all helium process is similar to that given in appendix C and will not be repeated in this section. We are again interested in predicting bubble collapse time as a function of initial bubble radius but now for bubbles maintained in a helium environment.

The helium pressure in the bubble is

$$P_B = P_o + \frac{2\gamma}{r_B} \quad (D1)$$

as in appendix C (eq. (C22)), but the helium partial pressure at the glass surface is now  $P(o, R) = P_o$ . Therefore, the pressure distribution becomes

$$P(z, R) = 2\gamma \left[ \frac{1}{\sqrt{R^2 + (d_s - z)^2}} - \frac{1}{\sqrt{R^2 + (d_s + z)^2}} \right] + P_o \quad (D2)$$

which is analogous to equation (C11). Equation (C14) for the pressure gradient is similarly changed so that the pressure  $P_B$  is replaced by  $2\gamma/r_B$  thus

$$\left( \frac{\partial P}{\partial z} \right)_{z=0} = \frac{4\gamma d_s}{(R^2 + d_s^2)^{3/2}} \quad (D3)$$

and

$$\dot{m}_B = - \frac{8\pi KMT_o\gamma}{V_o P_o T_B} \quad (D4)$$

Equations (C17) to (C24) remain unchanged, and equation (C26) becomes

$$\int_{r_B=r_{B,0}}^{r_{B,t}} \left( \frac{2}{3} r_B + \frac{P_o r_B^2}{2\gamma} \right) dr_B = -K \int_{t=0}^t dt \quad (\text{D5})$$

Carrying out the integration and evaluation at the limits results in

$$t = \frac{1}{3K} \left[ r_{B,0}^2 - r_{B,t}^2 + \frac{P_o}{2\gamma} (r_{B,0}^3 - r_{B,t}^3) \right] \quad (\text{D6})$$

and for bubble collapse to  $r_{B,t_c} = 0$

$$t_c = \frac{1}{3K} \left( r_{B,0}^2 + \frac{P_o r_{B,0}^3}{2\gamma} \right) \quad (\text{D7})$$

## REFERENCES

1. Kerslake, William R. : Accelerator Grid Tests on an Electron-Bombardment Ion Rocket. NASA TN D-1168, 1962.
2. Kerslake, William R. ; and Pawlik, Eugene V. : Additional Studies of Screen and Accelerator Grids for Electron-Bombardment Ion Thrusters. NASA TN D-1411, 1963.
3. Margosian, Paul M. : Preliminary Tests of Insulated Accelerator Grid for Electron-Bombardment Thrustor. NASA TM X-1342, 1967.
4. Nakanishi, S. ; Banks, B. A. ; and Richley, E. A. : High-Perveance Accelerator Grids for Low-Voltage Kaufman Thrusters. J. Spacecraft Rockets, vol. 5, no. 3, Mar. 1968, pp. 356-358.
5. Badger, Alfred E. : Glass Substantially Free From Bubbles. U.S. Patent 2,038,627, Apr. 28, 1936.
6. Jackson, John D. : Classical Electrodynamics. John Wiley & Sons, Inc., 1962, pp. 115-116.
7. Corson, Dale R. ; and Lorrain, Paul: Introduction to Electromagnetic Fields and Waves. W. H. Freeman and Co., 1962, p. 165.
8. Newkirk, Terry F. ; and Tooley, F. V. : Study of the Effect of Cation Concentration and Size on Helium Permeability of Alkali-silica Glasses. J. Am. Ceram. Soc., vol. 32, no. 9, Sept. 1949, pp. 272-278.
9. Rogers, W. A. ; Burtiz, R. S. ; and Alpert D. : Diffusion Coefficient, Solubility, and Permeability for Helium in Glass. J. Appl. Phys., vol. 25, no. 7, July 1954, pp. 868-875.
10. Banks, Bruce: Composite Ion Accelerator Grids. Paper presented at the Third International Conference on Electron and Ion Beam Science and Technology, Electrochemical Society of Boston, May 6-9, 1968.
11. Joos, George: Theoretical Physics. Third ed., Hafner Publishing Co., 1958, p. 224.

